

Nonlinearity in Single Photon Detection: Modeling and Quantum Tomography

Mohsen K. Akhlaghi,^{1,*} A. Hamed Majedi,¹ and Jeff S. Lundeen²

¹*Institute for Quantum Computing and ECE Department, University of Waterloo, 200 University Ave West, Waterloo, ON, Canada, N2L 3G1*

²*National Research Council - Institute for National Measurement Standards, 1200 Montreal Road, Ottawa, ON, Canada, K1A 0R6*

[*makeshava@maxwell.uwaterloo.ca](mailto:makeshava@maxwell.uwaterloo.ca)

Abstract: Single Photon Detectors are integral to quantum optics and quantum information. Superconducting Nanowire based detectors exhibit new levels of performance, but have no accepted quantum optical model that is valid for multiple input photons. By performing Detector Tomography, we improve the recently proposed model [M.K. Akhlaghi and A.H. Majedi, IEEE Trans. Appl. Supercond. **19**, 361 (2009)] and also investigate the manner in which these detectors respond nonlinearly to light, a valuable feature for some applications. We develop a device independent model for Single Photon Detectors that incorporates this nonlinearity.

© 2011 Optical Society of America

OCIS codes: (040.5570) Quantum detectors; (270.5570) Quantum detectors; (270.5585) Quantum information and processing.

References and links

1. L. A. Lugiato, A. Gatti, and E. Brambilla, "Quantum imaging," J. Opt. B: Quantum Semiclassical Opt. **4**, S176–S183 (2002).
2. M. W. Mitchell, J. S. Lundeen, and A. M. Steinberg, "Super-resolving phase measurements with a multiphoton entangled state," Nature **429**, 161–164 (2004).
3. J. T. Barreiro, T. C. Wei, and P. G. Kwiat, "Beating the channel capacity limit for linear photonic superdense coding," Nat. Phys. **4**, 282–286 (2008).
4. O. Daigle, C. Carignan, J. L. Gach, C. Guillaume, S. Lessard, C. A. Fortin, and S. Blais-Ouellette, "Extreme faint flux imaging with an emccd," Publ. Astron. Soc. Pac. **121**, 866–884 (2009).
5. R. K. Newsom, D. D. Turner, B. Mielke, M. Clayton, R. Ferrare, and C. Sivaraman, "Simultaneous analog and photon counting detection for raman lidar," Appl. Opt. **48**, 3903–3914 (2009).
6. E. Betzig, G. H. Patterson, R. Sougrat, O. W. Lindwasser, S. Olenych, J. S. Bonifacino, M. W. Davidson, J. Lippincott-Schwartz, and H. F. Hess, "Imaging intracellular fluorescent proteins at nanometer resolution," Science **313**, 1642–1645 (2006).
7. D. Achilles, C. Silberhorn, C. Sliwa, K. Banaszek, and I. A. Walmsley, "Fiber-assisted detection with photon number resolution," Opt. Lett. **28**, 2387–2389 (2003).
8. G. Puentes, J. S. Lundeen, M. P. A. Branderhorst, H. B. Coldenstrodt-Ronge, B. J. Smith, and I. A. Walmsley, "Bridging particle and wave sensitivity in a configurable detector of positive operator-valued measures," Phys. Rev. Lett. **102** (2009).
9. M. Michler, K. Mattle, H. Weinfurter, and A. Zeilinger, "Interferometric bell-state analysis," Phys. Rev. A **53**, R1209–R1212 (1996).
10. A. Ourjoumtsev, H. Jeong, R. Tualle-Broui, and P. Grangier, "Generation of optical 'schrodinger cats' from photon number states," Nature **448**, 784–786 (2007).
11. C. Xu, L. Mollenauer, and X. Liu, "Compensation of nonlinear self-phase modulation with phase modulators," Electron. Lett. **38**, 1578–1579 (2002).
12. R. H. Hadfield, "Single-photon detectors for optical quantum information applications," Nat. Photon. **3**, 696–705 (2009).

13. G. Goltsman, A. Korneev, O. Minaeva, I. Rubtsova, G. Chulkova, I. Milostnaya, K. Smirnov, B. Voronov, A. Lipatov, A. Pearlman, A. Cross, W. Slys, A. Verevkin, and R. Sobolewski, "Advanced nanostructured optical nbn single-photon detector operated at 2.0 k," *Prog. Biomed. Opt. Imag., Proc. SPIE* **5732**, 520–529 (2005).
14. A. D. Semenov, G. N. Gol'tsman, and A. A. Korneev, "Quantum detection by current carrying superconducting film," *Physica C* **351**, 349–356 (2001).
15. M. K. Akhlaghi and A. H. Majedi, "Semiempirical modeling of dark count rate and quantum efficiency of superconducting nanowire single-photon detectors," *IEEE Trans. Appl. Supercond.* **19**, 361–366 (2009).
16. G. N. Gol'tsman, O. Okunev, G. Chulkova, A. Lipatov, A. Semenov, K. Smirnov, B. Voronov, A. Dzardanov, C. Williams, and R. Sobolewski, "Picosecond superconducting single-photon optical detector," *Appl. Phys. Lett.* **79**, 705–707 (2001).
17. J. S. Lundeen, A. Feito, H. Coldenstrodt-Ronge, K. L. Pagnell, C. Silberhorn, T. C. Ralph, J. Eisert, M. B. Plenio, and I. A. Walmsley, "Tomography of quantum detectors," *Nat. Phys.* **5**, 27–30 (2009).
18. H. B. Coldenstrodt-Ronge, J. S. Lundeen, K. L. Pagnell, A. Feito, B. J. Smith, W. Mauerer, C. Silberhorn, J. Eisert, M. B. Plenio, and I. A. Walmsley, "A proposed testbed for detector tomography," *J. Mod. Opt.* **56**, 432–441 (2009).
19. J. L. F. X. Orgiazzi and A. H. Majedi, "Robust packaging technique and characterization of fiber-pigtailed superconducting nbn nano wire single photon detectors," *IEEE Trans. Appl. Supercond.* **19**, 341–345 (2009).
20. Z. Yan, M. K. Akhlaghi, J. L. Orgiazzi, and A. H. Majedi, "Optoelectronic characterization of a fiber-coupled nbn superconducting nanowire single photon detector," *J. Mod. Opt.* **56**, 380–384 (2009).
21. U. Leonhardt, *Measuring the Quantum State of Light* (Cambridge Univ. Press, 1997).
22. A. Feito, J. S. Lundeen, H. Coldenstrodt-Ronge, J. Eisert, M. B. Plenio, and I. A. Walmsley, "Measuring measurement: Theory and practice," *New J. Phys.* **11**, 093038 (2009).
23. S. Boyd and L. Vandenberghe, *Convex Optimization* (Cambridge Univ. Press, 2004).
24. G. Brida, L. Ciavarella, I. P. Degiovanni, M. Genovese, L. Lolli, M. G. Mingolla, F. Piacentini, M. Rajteri, E. Taralli, and M. G. A. Paris, "Full quantum characterization of superconducting photon counters," *arXiv:quant-ph:1103.2991* (2011).

1. Introduction

Single Photon Detectors (SPD) have been central to our exploration of the fundamental limits of imaging [1], interferometry [2], and communication [3]. They are used in astronomy [4], laser ranging [5], and biological imaging [6]. The SPD is a building block from which most more complicated optical detectors can be built. As examples, a photon number resolving detector can be built by multiplexing many SPDs [7], a phase sensitive detector by mixing the input light with an auxiliary laser beam [8], and an entanglement (i.e. Bell-state) detector by coincidence counting between SPDs behind a polarizing beamsplitter [9]. Consequently, SPDs have been ubiquitous in quantum optics and quantum information experiments performed up to this day.

Throughout, they have been described by a simple model. SPDs are binary detectors ('Click', or 'No Click'), and thus any non-zero number of detected photons will result in the same response: a Click. This behavior is contained within the standard model for the SPD's positive-operator-valued measure (POVM):

$$\pi_0^{SPD} = \sum_{n=0}^{\infty} (1 - P_1)^n |n\rangle\langle n|, \quad (1)$$

where π_0^{SPD} is the No Click operator, P_1 is the quantum efficiency, $|n\rangle$ is an n-photon state, and the Click operator is $\pi_1^{SPD} = 1 - \pi_0^{SPD}$. This simple model neglects the optical or electrical nonlinearities that likely exist, to some degree, in all SPDs. Nonlinear quantum optical detectors can prepare novel quantum optical states [10], characterize the photon statistics of input states [7], and measure the temporal profile of optical wavepackets through intensity autocorrelation [11]. Advanced SPDs, with their sophisticated structures [12], are good candidates to violate Eq. (1) through non-independent photoemissions and/or nonlinear gain mechanism.

A good example is Superconducting Nanowire SPDs (SNSPD), which, compared to conventional SPDs, offer higher maximum count rate, lower timing jitter, broader spectral range, and superior detection efficiencies at telecom wavelengths [12]. These detectors consist of a

meandering superconducting nanowire carrying a constant bias current close to their critical current. A single photon deposits enough heat to create a hotspot that is not superconducting. With the help of the bias current this can initiate a resistive bridge across the nanowire with some probability. The resulting voltage spike signals the detection of a single photon [13, 14]. Unfortunately, apart from such descriptions and calculations, there is no associated full quantum optical model (i.e. valid for multiple incident photons) from which we could formulate a general POVM for a single element SNSPD.

In an attempt to quantitatively describe the different observed experimental results within a single formalism, Akhlaghi and Majedi [15] proposed a semi-empirical model (AM model). In this model, the absorption of two or more photons at one point in the wire could result in cooperative resistive bridge formation. Hence, one might expect a nonlinear response in SNSPDs. Moreover, it might dominate the linear response at low bias currents. This is in agreement with the early experimental results on characterization of SNSPDs [16]. The model has been shown to work well with input light in a coherent state.

To further test this model we perform tomography on a SNSPD. Detector Tomography [17, 18] is an agnostic procedure to determine the POVM of a detector. The detector is treated as a Black Box in that we do not need to know its mechanism or make ancillary assumptions about it. Just recently demonstrated in principle, Detector Tomography has yet to be applied to a detector without an accepted model for its POVM.

2. Detector Tomography

To perform tomography we create a coherent state with a 1310nm laser that produces 200 ps pulses at 100 kHz. We use a programmable attenuator to set the coherent state amplitude, α . We sequentially send $R_T = 10^5$ copies of this state into the SNSPD system and record the number of detector Clicks, R_1 . This is repeated for a set of D states $\{|\alpha_i\rangle\}$, increasing α from $\alpha_0 = 0$ until the detector response is unchanging at α_D . i.e. $\partial R_1 / \partial \alpha = 0$. The estimated Click probability, R_1 / R_T , is equal to the Q-function of the Click POVM operator, $Q(\alpha)$. This, in itself, completely characterizes the detector response.

Our SNSPD consists of 4 nm thick by 120 nm wide Niobium Nitride meandering wire on sapphire. The active area is square with a fill factor of 60%. The SNSPD is coupled to an optical fiber and cooled down to 4.2K by exploiting a cryogenic setup (described in [19]). Fig. 1(a) shows a schematic of the measurement setup. The bias current is applied using a bias-Tee. The weak response of the SNSPD after amplification is split between an oscilloscope and a counter (see [20] for more detail). We use a 20ns counting gate, triggered by the laser, to reduce the dark count contribution from the times between input pulses.

We perform Detector Tomography (i.e. measure Q-function) at three bias currents, 25, 20, and 16 μ A. In Fig. 1(b), we plot the measured response for each of these (blue circles). We expect a standard linear SPD response at 25 μ A since this is the normal operation mode. Using Eq. (1), one expects a Q-function of the form $Q(\alpha) = 1 - \exp(-P_1|\alpha|^2)$. We estimate P_1 using a single data point at $Q(\alpha) = R_1 / R_T = 0.1$. Indeed, using this P_1 , the resulting predicted response (red line) agrees well with the measured response. Repeating this analysis for 20 and 16 μ A, we find that the estimated P_1 s, and thus, quantum efficiencies decrease as the bias current decreases. More significantly, the disagreement between the shape of the predicted and measured Click Probability distributions is substantial. Evidently, a SNSPD quickly becomes nonlinear as the bias current is lowered.

A general limitation of Q-functions is that they cannot be used to calculate a detector's response to arbitrary states of light [21]. Instead, one typically uses the POVM operators represented in the photon number basis. We find the SNSPD POVM by fitting it to the D measured statistics R_1 / R_T according to the methods given in [22]. Since the detector lacks phase sensi-

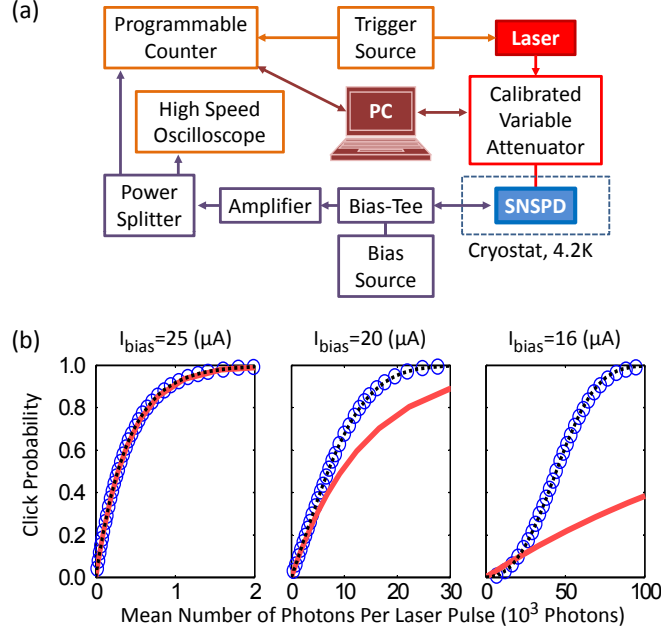


Fig. 1. (a) Schematics of the experimental setup. (b) Click Probability at different bias currents. The critical current was measured to be $26.0 \pm 0.5 \mu\text{A}$. The blue circles are measured Click probabilities (not all points are shown). The red lines are calculated using the linear model in Eq. (1) by calculating the efficiency parameter P_1 when the click probability is equal to 0.1. The black dotted lines are from the nonlinear SPD Model in Eq. (5). $\{P_n\}$ equals $\{7.30\text{e-}4, 2.49\text{e-}3\}$, $\{9.72\text{e-}6, 7.15\text{e-}5, 8.14\text{e-}9\}$, $\{0, 7.33\text{e-}8, 2.87\text{e-}10, 2.81\text{e-}14\}$ for 25, 20, and $16 \mu\text{A}$, respectively.

tivity, the off-diagonal elements of the Click operator are zero. We thus represent it as a vector Π (with dimensions $N \times 1$). We truncate Π at a number state $N - 1$ that is sufficiently high that $\Pi(N) \approx 1$.

One difference with [22] is that these particular SNSPDs have low system quantum efficiency (0.2% or less at 1310nm) and thus the maximum photon number, $N - 1$, required to span their response was large. Instead of using large matrices in the fitting, we scaled the inputs $\{|\alpha_i\rangle\}$ by a factor $k \ll 1$. For each bias current, k is chosen so that the Click Probability is 95% at an average photon number $\langle n \rangle = 30$. This scaled data is shown in Fig. 2(a) (black circles). We plot Π determined from it in Fig. 2(b) (blue circles). Using this Π , in Fig. 2(a) (blue line) we plot the predicted detector response to coherent input states. This fits the scaled data well, confirming the fitting procedure.

If scaled by too large a factor the POVM will, at the very least, be unrepresentative of the detector and, at worst, be physically impossible. Thus we test the estimated POVM for validity by adding k loss back into the POVM (i.e. $\Pi_{\text{unscaled}} = L^{-1} \Pi_{\text{scaled}}$, where L is the binomial distribution matrix described in [22]) and predicting the detector response to the original unscaled inputs, $\{|\alpha_i\rangle\}$. For all the bias currents, the difference between the predicted click probability and the raw data (i.e. $|R_1/R_T - \text{Tr}[\Pi_{\text{unscaled}} |\alpha_i\rangle \langle \alpha_i|]|$) is less than 0.15% on average and has a maximum of 1.4%. This indicates that we have accurately estimated the SNSPD POVM using the scaling technique.

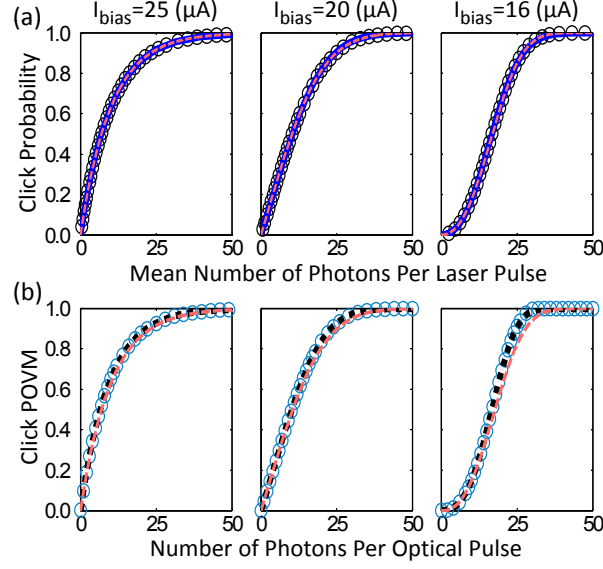


Fig. 2. (a) The Q-function (i.e. click probability for coherent state inputs) of the scaled detector at different bias currents. The raw scaled data (black circles) agrees well with the tomographic POVM (blue line) and the AM Model (red dashed line). (b) The corresponding Click POVM operator. The operator found from tomography (blue circles) disagrees with that from the AM Model (red dashed line) but agrees with that from the nonlinear SPD Model (black dotted line). In the latter, $\{P_n\}$ equals $\{7.29\text{e-}4, 9.95\text{e-}2\}$, $\{1.08\text{e-}5, 4.76\text{e-}2, 3.74\text{e-}3, 1.13\text{e-}4\}$, $\{0, 1.97\text{e-}4, 2.01\text{e-}3, 4.87\text{e-}4, 5.07\text{e-}5\}$ for 25, 20, and $16\mu\text{A}$, respectively.

3. Generalized Model

The lack of ancillary assumptions and models in Detector Tomography make it general and objective. At the same time, it provides a surplus of information (i.e. $O(N)$ parameters) that can be difficult to interpret. Tomography can hardly replace the natural ease and intuition that is associated with a model. A good model candidate is the AM model. Indeed, plotting the AM model in Fig. 2(a) (red dashed line) shows that it can be fit to the scaled data.

To find an analytic expression for the SNSPD POVM in the number state basis we repeated the derivation of the AM model given in [15] with one change: We derived the detector response to a Fock state rather than a coherent state input. The parameter values in the model should remain the same in either case. Thus, using the parameter values from the AM model curves in Fig. 2(a) we plot the AM POVM in Fig. 2(b) (red dashed line). Substantial disagreement between the tomographic POVM and the AM POVM suggests there is an error.

Indeed, further investigation revealed that in Eqs. (4) and (5) in [15] the average photon number is used in place of the actual photon distribution. The resulting error is only revealed in the comparison of analytical and tomographic POVMs. We fixed this error and found that the resulting analytic POVM has a form that is applicable to general SPD detectors. Leaving behind the SNSPD specific derivation in [15], we now introduce a broad detector model that is able to describe nonlinear SPDs. We do this by generalizing Eq. (1) to multiphoton detection.

Consider a binary detector that is only sensitive to n number of photons; any less and the detector responds with No Click, any more and it still only outputs one Click. This is the n -photon generalization of the SPD and, hence, we call it an n -photon detector (NPD). If $m > n$

photons impinge on the detector, there are m choose n ways for those m photons to trigger the NPD. Consequently the generalization of Eq. (1) is:

$$\pi_0^{NPD} = \sum_{m=0}^{\infty} (1 - P_n)^{\binom{m}{n}} |m\rangle \langle m|, \quad (2)$$

where π_0^{NPD} is the No Click operator, P_n is the n -photon detection efficiency and $\binom{m}{n}$ is the binomial coefficient ($= 0$ for $n > m$, $= 1$ for $n = 0$). This generalization works even for a zero photon detector. We can identify P_0 as what is commonly called the ‘dark count probability’.

A nonlinear SPD can be modeled as concurrent NPDs. As shown in Fig. 3(a), the model consists of a logical OR between M NPDs, where M represents the maximum number of mechanisms that should be present in order to describe the response of the detector before it saturates at high intensities. The associated POVM operators are:

$$\pi_1^{NL} = 1 - \sum_{m=0}^{\infty} \prod_{n=0}^{M-1} (1 - P_n)^{\binom{m}{n}} |m\rangle \langle m|, \quad (3)$$

for Click and $\pi_0^{NL} = 1 - \pi_1^{NL}$ for No Click. The Click probability of the nonlinear SPD in response to a coherent state $|\alpha\rangle$ is:

$$P_{Click}(\alpha) = 1 - \sum_{m=0}^{\infty} e^{-|\alpha|^2} \frac{|\alpha|^{2m}}{m!} \prod_{n=0}^{M-1} (1 - P_n)^{\binom{m}{n}}. \quad (4)$$

This can be rewritten in matrix form as:

$$C = F\Pi = F(E - \exp(GH)), \quad (5)$$

where C (with dimensions $D \times 1$), includes the D measured statistics, R_1/R_T ; Π ($N \times 1$) includes the diagonal elements of π_1^{NL} ; F contains the D coherent state probes, $F_{i,j} = |\alpha_i|^{2j} \exp(-|\alpha_i|^2) / j!$; E is a matrix of ones; G is a matrix of binomial coefficients such that $G_{i,j} = \binom{j-1}{i-1}$; and H ($M \times 1$) is an unknown matrix which includes the unknown set $\{P_n\}$, $H_{i,1} = \ln(1 - P_{n=i-1})$.

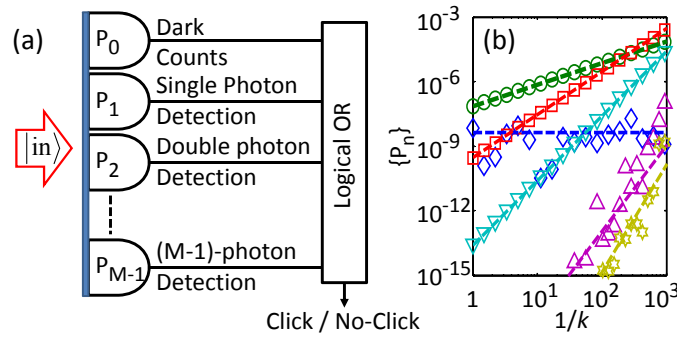


Fig. 3. (a) The Nonlinear Single Photon Detector model. Each element represents an n -Photon Detector. A broadly applicable model is created by logically ORing these elements. (b) $\{P_n\}$ at $16\mu A$ found under different scaling factors, k . \diamond , \circ , \square , ∇ , \triangle , and \star represent $P_{n=0}$ to $P_{n=5}$ respectively. The dotted lines have slopes equal to n . The plot shows a linear optical loss of η scales $P_n \rightarrow \eta^n P_n$.

We estimate H by solving the following constrained nonlinear multivariable optimization problem:

$$\min \left\| \frac{C - FE + F \exp(GH)}{C} \right\|_2, \quad (6)$$

subject to $H \leq 0$. The second norm of a matrix is defined as $\|A\|_2 = \left(\sum_{i,j} |A_{i,j}|^2 \right)^{1/2}$. Each element of the expression is normalized to C to give equal weighting to all the points. The constraint of the problem ensures the optimization leads to a physical result for the set $\{P_n\}$. We note the function $\exp(\alpha x)$ is convex on \mathbb{R} for any $\alpha \in \mathbb{R}$ [23], which also makes Eq. (6) convex.

We first solve Eq. (6) for scaled input states. From the estimated $\{P_n\}$ we only keep those elements that change the minimum of Eq. (6) by more than 1% ($25\mu\text{A}$: $\{P_0, P_1\}$; $20\mu\text{A}$: $\{P_0, \dots, P_4\}$; $16\mu\text{A}$: $\{P_1, \dots, P_4\}$). These parameters classify the operation of the SNSPD, from a standard SPD at $25\mu\text{A}$ to a composite of one, two, three, and four photon detectors at $16\mu\text{A}$.

From these $\{P_n\}$ we calculate the nonlinear SPD Click POVM operator for the three bias currents in Fig. 2(b) (black dotted line). They agree with the tomography POVMs to within 1% for most of the elements of Π . For $25\mu\text{A}$ and $20\mu\text{A}$ the maximum difference is 3% at $\Pi(n=1)$ and 6% at $\Pi(n=3)$ for $16\mu\text{A}$. This excludes the large error at $\Pi(n=0)$, which we attribute to insufficient measured statistics at extremely small mean photon numbers. The Quantum Fidelity (see [22] for a definition) of the model and tomography operators are above 99.8% for all three bias currents. Thus, the model successfully gives the POVM of the SNSPDs including their nonlinearity, but with a dramatic reduction in the number of parameters compared to tomography.

We can attribute the SNSPD nonlinearity to the fact that at lower bias currents the absorption of multiple photons in close proximity and within a short period of time can inject enough energy to switch the wire to normal state more efficiently than independent absorptions.

In Fig. 1(b), we plot the model's predicted response to the coherent state inputs, with parameters from the unscaled data (black dotted line). The difference with the measured statistics is less than 0.34% on average (i.e the minimum found in Eq. (6) divided by the number of points).

Unlike the standard SPD, where $P_1 \rightarrow \eta P_1$ under a preceding optical loss of η , there is no analytic formulae for how $\{P_n\}$ transform under loss. By inspection of the scaled and non-scaled model fits (see Fig. 3(b)), however, each element of $\{P_n\}$ that is significant approximately scales as η^n . So removing any linear optical inefficiency from a nonlinear photon counter makes it more nonlinear. We also note P_0 is not dependent on the optical input as expected.

4. Conclusion

The almost identical outcome of Detector Tomography and the nonlinear SPD model confirms both of them are reliable. This is a good example of how Detector Tomography is particularly useful for characterizing detectors outside their normal operating regime, where there is no model for their operation. We expect the nonlinear SNSPD model to be useful for other nonlinear binary detectors such as two-photon absorbing Avalanche Photodiodes and Electron Multiplying CCDs (thresh-helded). It will also be useful for characterizing conventional SPDs and putting limits on their nonlinearity.

Acknowledgments

Recently, a preprint of a related paper has appeared [24]. We acknowledge the financial support of NSERC and BDC. We also acknowledge Jean-Luc F. Orgiazzi for development of the cryogenic setup.